JMEPEG (2004) 13:691-699
DOI: 10.1361/10599490421321

1059-9495/$19.00

Finite Element Modeling and Optimization of Superplastic Forming Using Variable Strain Rate Approach

Mohammad A. Nazzal, Marwan K. Khraisheh, and Basil M. Darras

(Submitted August 23, 2004)

Detailed finite element simulations were carried out to model and optimize the superplastic blow forming process using a microstructure-based constitutive model and a multiscale deformation stability criterion that accounts for both geometrical instabilities and microstructural features. Optimum strain rate forming paths were derived from the multiscale stability analysis and used to develop a variable strain rate forming control scheme. It is shown that the proposed optimization approach captures the characteristics of deformation and failure during superplastic forming and is capable of significantly reducing the forming time without compromising the uniformity of deformation. In addition, the effects of grain evolution and cavitation on the superplastic forming process were investigated, and the results clearly highlight the importance of accounting for these features to prevent premature failure.

Keywords cavitation, finite element modeling, grain growth, optimization, superplastic forming

1. Introduction

Superplastic forming (SPF) is a near-net-shape forming process used with superplastic materials, a unique class of metals that has the ability to undergo extraordinarily large tensile deformation. Although SPF has many advantages over conventional forming operations, especially cost and weight saving potentials, its industrial use is still limited (Ref 1). For the SPF technique to become acceptable as an efficient forming process and to facilitate its use in higher volume applications, a comprehensive numerical predictive tool that can design and simulate the various aspects of the SPF process must be developed. To achieve that goal, a number of important issues that currently hamper the widespread use of SPF must be solved. The most critical issues are related to material behavior during forming and include low production rate, due to low deformation rates used, and limited predictive capabilities of material deformation and failure.

Gas forming is considered the most common practice used in forming superplastic materials where the sheet is formed onto the die using pressurized gas. This process received considerable attention from researchers and was investigated experimentally, analytically, and using finite element (FE) simulation, see for example Ref 2 to 9. Generally, these studies have limited capabilities of predicting the thinning of the formed parts. The selection of the forming pressure profile is very critical as it ultimately determines the integrity of the formed part and the production time. Forming pressure profiles used in the industry are usually based on trial and error and typically use low "safe" pressure to prevent premature failure. The challenge is to develop optimum forming pressure profiles that can reduce the forming time and maintain the integrity of the formed part.

The main scheme usually used to optimize the SPF process is to maintain the strain rate during forming to an optimum range, where maximum ductility is achieved. This may prevent thinning and premature failure, but would not reduce the forming time, since the optimum strain rate is usually low.

Recently, it has been reported that using pressure profiles based on variable strain rate schemes may reduce the forming time and maintain the integrity of the formed component. Ding et al. (Ref 6) analyzed the superplastic blow forming of a thin superplastic sheet into a rectangular box using a two-dimensional (2-D) FE model. They reported that a variable strain rate control scheme is an efficient technique for superplastic blow forming. Their 2-D FE model, however, concluded that the localized thinning occurs in the die entry region, whereas the localized thinning occurs elsewhere when forming three-dimensional (3-D) deep components. Experimentally, Khraisheh and Zbib (Ref 8) proposed an optimum forming pressure profile based on variable strain rates for free blow forming of Pb-Sn superplastic sheet materials. The results clearly showed significant improvements: Not only was the integrity of the formed part maintained, but the forming time was also reduced with a comparable amount of deformation. This approach, however, was based on experimental observations, and its application to other materials may be limited since it was not based on analytical considerations.

Variable strain-rate-based pressure profiles for complex geometries can be generated using finite element analysis (FEA). However, to develop accurate and optimum profiles, the deformation behavior of superplastic materials must be accurately described during forming and an accurate failure criterion must be used. Most of the available FE analyses use simple constitutive models, usually built in the software, and do not take the

This paper was presented at the International Symposium on Superplasticity and Superplastic Forming sponsored by the Manufacturing Critical Sector at the ASM International AeroMat 2004 Conference and Exposition, June 8-9, 2004, in Seattle, WA. The symposium was organized by Daniel G. Sanders, The Boeing Company.

Mohammad A. Nazzal, Marwan K. Khraisheh, and **Basil M. Darras,** Center for Manufacturing and Department of Mechanical Engineering, University of Kentucky, Lexington, KY 40506-0108. Contact e-mail: khraisheh@engr.uky.edu.

characteristics of superplastic materials into account. Additionally, none of the available studies account for both cavitation and necking when studying the failure of superplastic materials.

In this work, the authors used a recently developed microstructure-based constitutive model (Ref 10) with a multiscale failure criterion (Ref 11, 12) incorporated into a general FE model to optimize the superplastic forming process. The focus of this work was the implementation of the deformation and failure models into FEA and the development of an optimization scheme based on the multiscale failure criterion. A brief overview of the constitutive model and the stability criterion is first given followed by detailed FEA and optimization.

2. Constitutive Equations

The constitutive model used in this study is based on the continuum theory of viscoplasticity with internal variables. Details on the development of the model are given elsewhere (Ref 10, 13). The simplified one-dimensional (1-D) form of this model is given by:

$$\dot{\varepsilon} = \frac{C_i}{d^p}\left[\left(\frac{\sigma}{\{1-f_a\}}\right) - \sigma_o\right]^{1/m} + C_{ii}\left[\frac{\sigma}{\{1-f_a\}}\right]^n \quad \text{(Eq 1)}$$

where $\dot{\varepsilon}$ is the strain rate, σ is the flow stress, σ_o is the threshold stress, m is the strain rate sensitivity, n is the stress exponent, p is the grain growth exponent, d is the average grain size, f_a is the area fraction of voids, and C_i and C_{ii} are material constants.

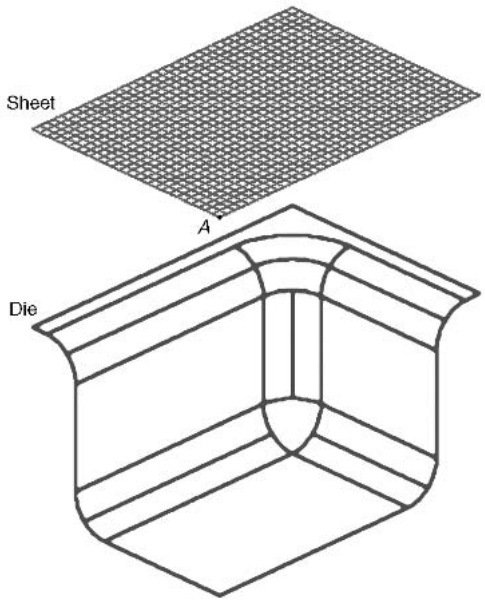

Fig. 1 Die-sheet geometry for the superplastic gas-blow forming of a rectangular box

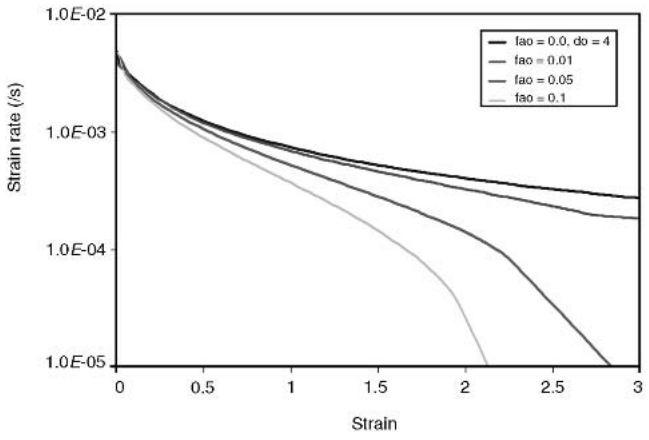

Fig. 2 Optimum forming paths for different initial void area fractions

2.1 Grain Growth Model

To account for grain growth during superplastic deformation, an evolution equation for d in Eq 1 is used. The grain growth model used in this analysis is similar to the one used by Hamilton et al. (Ref 14), where both static ($\dot{d}_s$) and dynamic ($\dot{d}_D$) grain growths are taken into account. The resulting total grain growth rate is given by:

$$\dot{d} = \dot{d}_s + \dot{d}_D = \frac{k_s}{d^g} + \frac{k_d}{d^g}\left[1 - \exp\left(\frac{-t}{\tau}\right)\right]\dot{\varepsilon} \quad \text{(Eq 2)}$$

where t is the time, and k_s, g, k_d, and τ are material constants.

2.2 Void Growth Model

Similarly, an evolution equation for the area fraction of voids f_a that appears in Eq 1 is used to account for cavitation and damage evolution. Due to the large deformation associated with superplastic forming, the controlling void growth mechanism is believed to be plastically controlled (Ref 15). As a result, the area fraction of voids is exponentially related to the plastic strain:

$$f_a = f_{a_o} \exp(\psi\varepsilon) \quad \text{(Eq 3)}$$

where f_a is the initial area fraction of voids, and ψ is a material parameter that depends on the strain rate sensitivity index m. Nucleation of cavities is not included in this analysis.

3. Multiscale Stability Criterion

The amount of stable and uniform deformation is limited by the onset of localized thinning (geometrical necking) and cavitation (microstructure evolution). The contribution of cavitation and necking to the overall deformation instability depends on material and process parameters. Available studies on failure during superplastic deformation considers only one failure mode, and there are no studies that examine the combined

effects of both failure modes. The condition for stable plastic deformation as defined by Hart (Ref 16) is given by:

$$\left(\frac{d\dot{A}}{dA}\right) \leq 0 \qquad \text{(Eq 4)}$$

where $d\dot{A}$ is the variation in the area increment rate and dA is the variation in cross-sectional area. Assuming that stress is a function of strain and strain rate only (not accounting for microstructure evolution), Hart derived a stability criterion for the uniaxial loading case, which has the form:

$$\gamma + m \geq 1 \qquad \text{(Eq 5)}$$

where γ is the strain rate hardening exponent and m is the strain rate sensitivity index. Incorporating the modified constitutive Eq 1 along with the evolution Eq 2 and 3 into the framework of Hart's analysis, a new stability criterion accounting for both geometrical instabilities and microstructure aspects was developed (Ref 12), which at the onset of instability has the form:

$$\gamma' + m' + \zeta = 1 \qquad \text{(Eq 6)}$$

in which case:

$$\gamma' = \frac{\dot{d}}{\dot{\varepsilon}}\left(\frac{\partial \dot{\varepsilon}}{\partial d}\right)_{\sigma, f_a}, m' = \frac{\sigma}{\dot{\varepsilon}}\left(\frac{\partial \dot{\varepsilon}}{\partial \sigma}\right)_{\sigma, f_a}, \zeta = \frac{\psi f_a}{\dot{\varepsilon}}\left(\frac{\partial \dot{\varepsilon}}{\partial f_a}\right)_{\sigma, d}$$

where γ' represents strain hardening due to grain coarsening, m' represents strain rate sensitivity, and ζ represents the influence of cavitation. Equation 6 reduces to Eq 5 when microstructure evolution is not considered.

4. Finite Element Analysis

The FE simulation has been performed using a commercial FE package, ABAQUS version 6.3. This FE code includes direct implicit integration, which is chosen for superplastic analysis since it enables a full static solution of deformation problems with convergence control. In addition, the time increment size can be defined with practical limits. In explicit dynamic software, on the other hand, the stability requirement forces the time step to be very small, and the total number of steps for complete analysis can run into thousands of steps. Thus, for the superplastic forming process, which is usually slow, static implicit software is the best choice compared with explicit dynamic software.

First, a deep rectangular box geometry is used to investigate various forming scenarios to arrive at an optimum forming procedure. Then, the results are used to simulate the superplastic forming of an aircraft blowout door to verify the capability of the optimization scheme. Figure 1 shows the die-sheet geometry for simulating superplastic forming of a sheet into a rectangular box. The final dimensions of the box are 60 cm long by 40 cm wide by 20 cm deep with a 2 cm flange around it. The initial dimensions of the blank are 64 by 44 cm, and the thickness is 0.3175 cm. This geometry is chosen due to its simplicity yet its ability to represent superplastic forming effectively due to the large deformation involved.

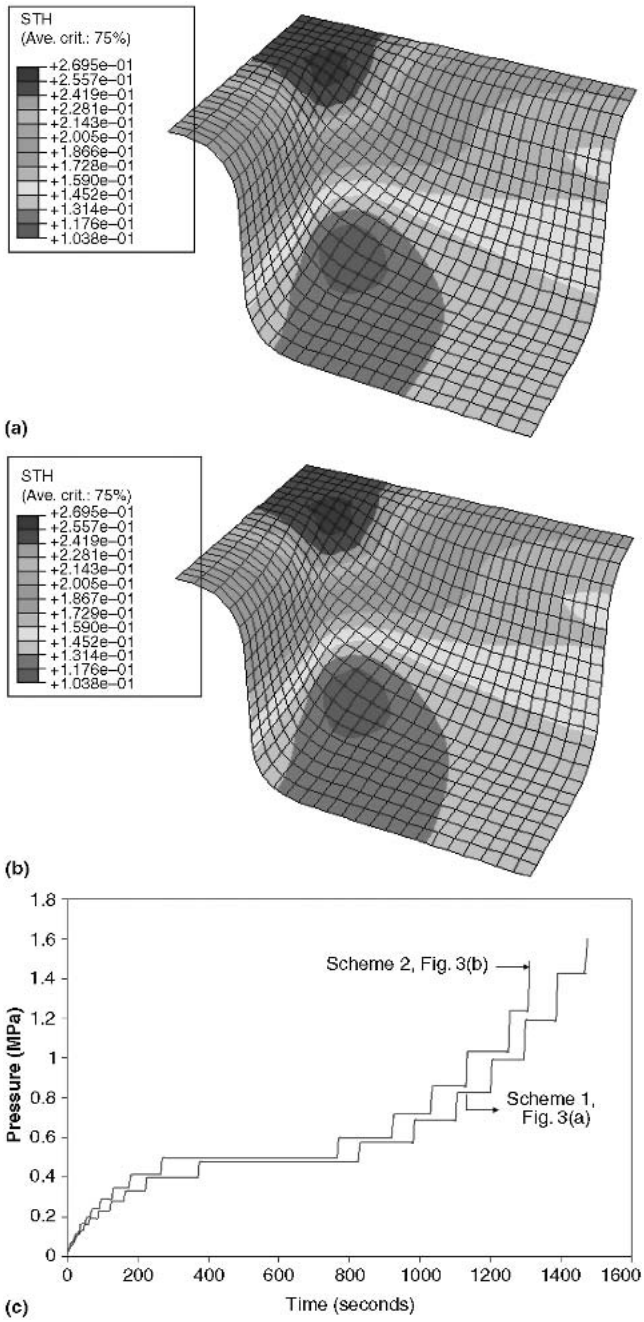

Fig. 3 Comparison between Scheme 1 (maximum global constant strain rate control) and Scheme 2 (maximum local constant strain rate control). (a) Thickness distribution profile for Scheme 1 (forming time 1480 s). (b) Thickness distribution profile for Scheme 2 (forming time 1311 s). (c) Pressure profiles

Due to symmetry, a quarter of the blank is modeled using 704 fully integrated bilinear membrane elements. However, more than a quarter of the die has been modeled using 231 triangular rigid elements to avoid the sheet material falling off the die surface during the analysis. The isotropic Coulomb friction model provided by ABAQUS with a friction coeffi-

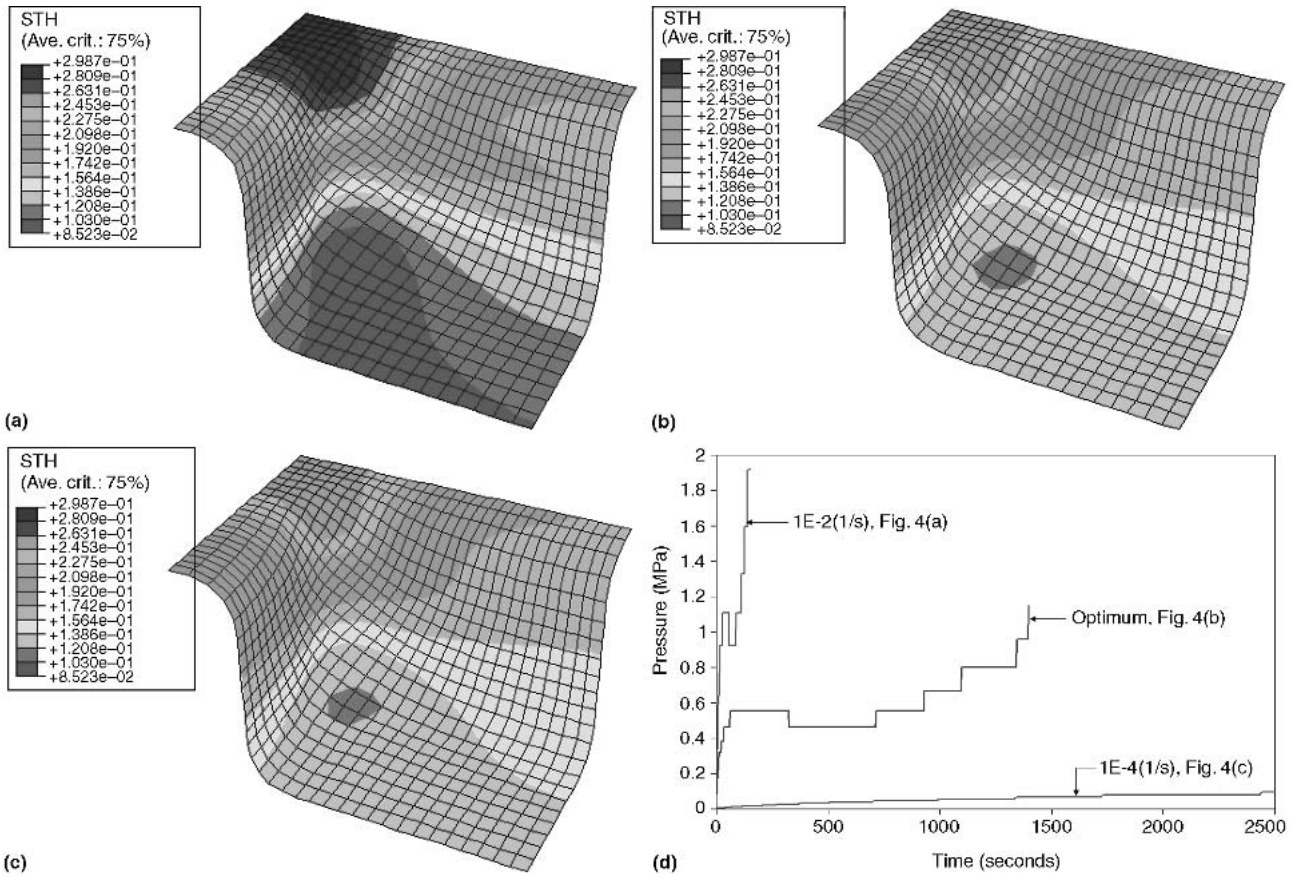

Fig. 4 Comparison between Scheme 2 (maximum local constant strain rate control) and Scheme 3 (maximum local variable strain rate control). (a) Thickness distribution profile for $\dot{\varepsilon} = 1 \times 10^{-2}$ s^{-1} (forming time 160 s). (b) Thickness distribution profile for the optimum case (forming time 1400 s). (c) Thickness distribution profile for $\dot{\varepsilon} = 1 \times 10^{-4}$ s^{-1} (forming time 14130 s). (d) Pressure profiles

cient $\mu = 0.1$ is used to account for surface interaction between the die and the sheet. The forming process is considered complete when all the nodes on the sheet are in full contact with the die.

4.1 Constitutive Equations Implementation in the FE Code

Two user-defined subroutines were developed to define the material viscoplastic behavior and the initial solution-dependent state variable fields at particular material points. The constitutive equations are implemented in ABAQUS through the user subroutine CREEP, which is called at all integration points during the viscoplastic analysis. The accuracy of numerical integration is controlled by setting the ABAQUS parameter CETOL equal to 0.1%. This parameter is defined by choosing an acceptable stress error tolerance and dividing it by the elastic modulus. This way, the accuracy is checked by comparing the equivalent creep strain rate at the beginning and the end of each increment. The difference should be less than CETOL divided by the time increment. Otherwise, the increment is reattempted with a smaller time increment. Solution-dependent variables such as grain growth and cavitation are initialized using the SDVINI subroutine and their evolution is calculated within the CREEP subroutine.

5. Forming Control Schemes

One of the critical aspects of superplastic forming analysis is to determine the pressure time history required to form the component as fast as possible without exceeding a specified optimum superplastic strain rate in the material. This is accomplished by using an ABAQUS built-in algorithm that works as follows. During each increment, the ratio (r) of the maximum equivalent creep strain rate ($\dot{\varepsilon}_{max}$) to the target creep strain rate ($\dot{\varepsilon}_{tar}$) found in the specified element set is calculated:

$$r = \frac{\dot{\varepsilon}_{max}}{\dot{\varepsilon}_{tar}}$$

Now if $0.2 \leq r \leq 3.0$, the increment is accepted and the pressure is adjusted:

If $0.2 \leq r < 0.5$ then $P_{new} = 1.5P_{old}$

If $0.5 \leq r < 0.8$ then $P_{new} = 1.2P_{old}$

If $0.8 \leq r < 1.5$ then $P_{new} = P_{old}$

If $1.5 \leq r \leq 3.0$ then $P_{new} = 0.834P_{old}$

where P_{new} is the new pressure magnitude and P_{old} is the old pressure magnitude.

However, if $r < 0.2$, or $r > 3.0$, in any given increment, the increment is abandoned and restarted according to:

If $r < 0.2$ then $P_{new} = 2P_{old}$

If $r > 3.0$ then $P_{new} = 0.5P_{old}$

Based on this algorithm, three different schemes to control the loading schedule during the forming process were investigated.

5.1 Scheme 1: Maximum Global Constant Strain Rate Control

In this scheme, the loading is controlled on the basis of the maximum equivalent creep strain rate found in the whole sheet. In the initial stages of deformation, where the material is formed under free bulging, the maximum strain rate occurs at the middle of the sheet (point A, Fig. 1). However, when point A makes contact with the die, the maximum strain rate starts shifting toward the regions that are not in contact with the die until the bottom corners of the box are entirely filled.

5.2 Scheme 2: Maximum Local Constant Strain Rate Control

After running the simulation using Scheme 1, it was observed that both the maximum localized thinning and the maximum strain in the sheet occur at the bottom corner of the box. As a result, the sheet elements that lie in this critical region were tracked, and the analysis was rerun such that the pressure is controlled on the basis of the maximum equivalent creep strain rate found in the critical region of the sheet only.

5.3 Scheme 3: Proposed Optimization Technique: Maximum Local Variable Strain Rate Control

This scheme is based on an optimum strain rate path obtained from the multiscale stability criterion described in Section 3 of this article. This path is generated by solving Eq 6 along with Eq 1 to 3 numerically for different strain rates to yield critical strains at the onset of instability. The optimum strain rate path is shown in Fig. 2 for Ti-6Al-4V superplastic material at 900 °C. The pressure is controlled on the basis of a maximum variable equivalent creep strain rate found in the critical region mentioned in Scheme 2 (Section 5.2).

6. Discussion and Results

The simulations were carried out for Ti-6Al-4V superplastic material at 900 °C. The procedure presented here, however, is general and can be applied to other superplastic materials if experimental data are available to obtain the material parameters used in the constitutive model and the stability criterion. The material parameters for Ti-6Al-4V used in the simulation are listed in Table 1. These parameters were obtained by fitting various experimental data obtained from Hamilton et al. (Ref 14) and Johnson et al. (Ref 17) to the models used here.

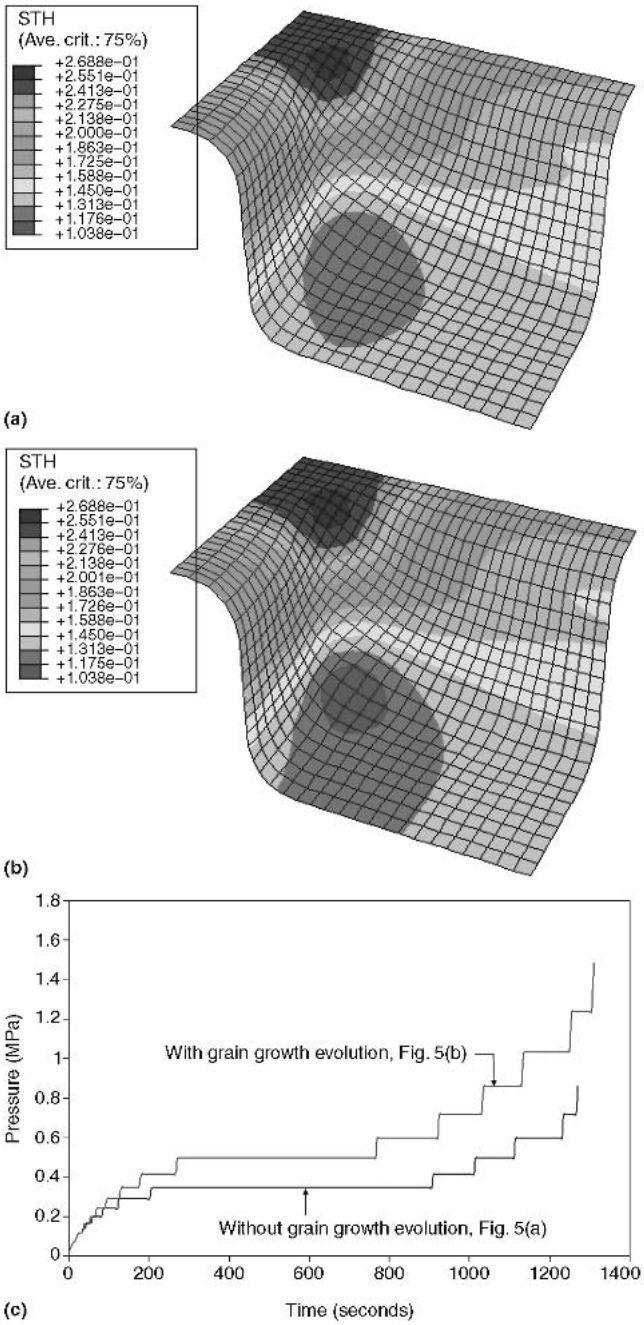

Fig. 5 Grain growth effects. (a) Thickness distribution profile without taking microstructure evolution into account (forming time 1270 s). (b) Thickness distribution profile taking microstructure evolution into account (forming time 1311 s). (c) Pressure profiles

6.1 Comparison of Control Schemes

To investigate the differences among the forming control schemes, a number of simulation runs were carried out using the same set of geometrical and material parameters. For these simulations, the grain growth effect is taken into account, but no cavitation is considered.

6.1.1 Comparison Between Schemes 1 and 2. Figure 3(c) shows the pressure profiles for the two schemes. Scheme 1 is

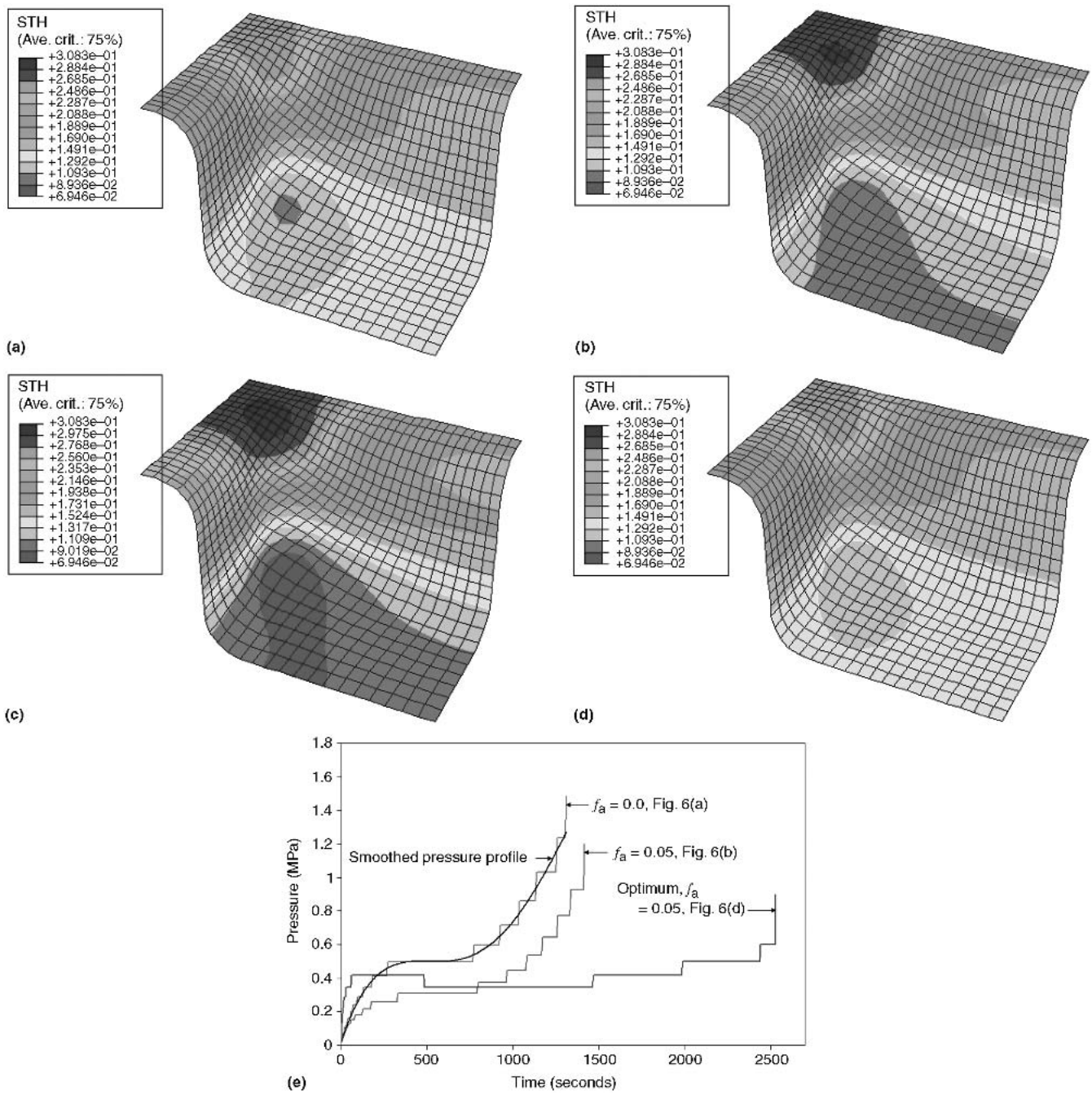

Fig. 6 Cavitation effects. (a) Thickness distribution profile without taking cavitation into consideration $f_{a_o} = 0.0$ (forming time 1311 s). (b) Thickness distribution profile taking cavitation into consideration $f_{a_o} = 0.05$ (forming time 1420 s). (c) Thickness distribution profile using the pressure-time history generated from case (a) in a model that accounts for cavitation $f_{a_o} = 0.05$ (forming time 1311 s). (d) Thickness distribution profile for the optimum case (forming time 2530 s). (e) Pressure profiles

the maximum global constant strain rate control, and Scheme 2 is the maximum local constant strain rate control. In this case, a maximum equivalent constant strain rate, $\dot{\varepsilon} = 1 \times 10^{-3}$ s^{-1}, was used. It is observed that the forming time for Scheme 2 is 11.1% less than that for Scheme 1. When comparing Fig. 3(a) and (b), it can be deduced that the localized thinning is almost the same for both schemes. Since the difference in the sheet thickness distribution is not significant, and 11.1% of the forming time is saved using Scheme 2, it was concluded that Scheme 2 is more effective than Scheme 1.

6.1.2 Comparison Between Schemes 2 and 3. The thickness distributions and pressure profiles for two different target strain rates of 1×10^{-2} and 1×10^{-4} s^{-1} using Scheme 2, and for the optimum variable strain rate (Scheme 3), are shown in Fig. 4. It is observed that the sheet formed at the lowest strain rate (1×10^{-4} s^{-1}) shows the most uniform thickness distribu-

tion and the minimum localized thinning. However, it took 14,130 s to form the component. On the other hand, the sheet formed using a maximum strain rate of 1×10^{-2} s^{-1} was done in 160 s. However, the thickness distribution is nonuniform and the localized thinning is so severe that premature rupture might occur at the corner of the box. Using the optimum pressure profile, the forming time was 1400 s, significantly reduced from 14,130 s, and the uniformity of the sheet thickness is maintained and compares very well with the one obtained using a target strain rate of 10^{-4} s^{-1}. It is seen from Fig. 4(d) that higher gas pressure is required for higher target strain rates. This is due to higher flow stress associated with the higher strain rate. The proposed optimization scheme based on the multiscale stability criterion clearly demonstrated its advantages by significantly reducing the forming time and maintaining a uniform thickness distribution of the formed part.

6.2 Effects of Grain Growth

To investigate the effect of grain growth, two simulation runs were conducted (cavitation is not accounted for). Scheme 2 is employed using a maximum equivalent strain rate of 1×10^{-3} s^{-1}. For both runs, the initial grain size is set to $d_o = 4$ μm. In the first simulation, grain growth is not taken into account and the average grain size appearing in Eq 1 is set to a constant value of 4 μm. During the second run, the grain size is updated during deformation according to Eq 2. Figure 5 shows the influence of grain growth on the pressure-time history and thickness distribution. It is interesting to note that accounting for grain growth requires higher forming pressure than the pressure needed to form the material if grain growth is not accounted for. This can be explained by the fact that grain growth leads to a hardening effect and an increase in the flow stress needed to deform the material (Eq 1). Since most superplastic materials exhibit grain growth, the results highlight the importance of accounting for grain growth. In addition, greater localized thinning is observed when grain growth is taken into account due to the higher flow stress.

6.3 Effects of Cavitation

One of the main advantages of the constitutive model implemented in the simulations is that it takes cavitation and its evolution into consideration. Therefore, the effect of cavitation is studied in detail in this work. Four simulation tests were performed to demonstrate the effect of cavitation on the forming process. The grain growth effect is taken into account for the four simulation tests. In the first test, the analysis was run using Scheme 2, assuming that the material does not exhibit cavitation. In other words, the initial fraction of voids is set equal to zero. In the second test, all material and simulation parameters remain the same except that the initial fraction of voids is set to $f_{a_o} = 0.05$. The results are shown in Fig. 6(a), (b), and (e). It is seen that the pressure magnitude decreases for the same forming time when cavitation is taken into account. However, the total forming time increases by 9.1%. This result is expected since the component undergoes more thinning when considering cavitation. Thus, the pressure decreases and the forming time increases to avoid exceeding the maximum target strain rate in the forming region. To emphasize the effect of cavitation, a third simulation run is conducted. In this test, the pressure profile generated in the first simulation run (no cavitation), which is shown in Fig. 6(e), is used to form a sheet that exhibits cavitation with an initial area void fraction of $f_{a_o} = 0.05$. The results of the third run are shown in Fig. 6(c). It is clearly demonstrated that cavitation has a drastic effect on the thickness distribution. The formed part in the third run undergoes severe localized thinning when compared with the distribution shown in Fig. 6(a). The third simulation run represents a scenario often seen in the industry. A forming pressure profile based on a simple constitutive model that does not account for cavitation is used to form a sheet that most likely will undergo cavitation. This may explain the current limited predictive capabilities of the available models. To overcome the severe localized thinning resulting from cavitation, the optimum variable strain rate path, shown in Fig. 2, is used in the fourth simulation run. The results of this run are shown in Fig. 6(d) and (e). Although it took 2530 s to form the component using the optimum variable strain rate path, the thickness distribution is improved significantly. It took more time because the optimum procedure is designed such that slower forming is used to avoid thinning caused by both necking and cavitation. The proposed optimum approach acts as a smart control that adjusts the forming pressure according to the actual material behavior during deformation. Initially when cavitation is not significant, the forming pressure is high, and as deformation

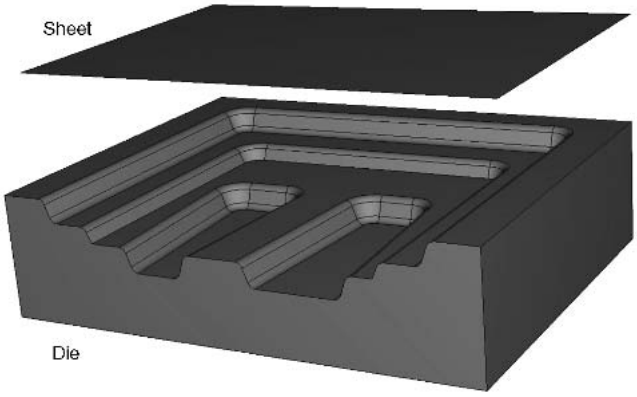

Fig. 7 Die-sheet geometry for simulating superplastic gas-blow forming of an aircraft blowout door

Table 1 List of material parameters used in the simulations

Material parameter	Value
σ_o	25 N/cm^2
m	0.7
n	4.3
p	3
C_i	1.3×10^{-18}
C_{ii}	2.2×10^{-19}
k_s	0.042
k_d	939
g	3.9
τ	1300
ψ	0.8

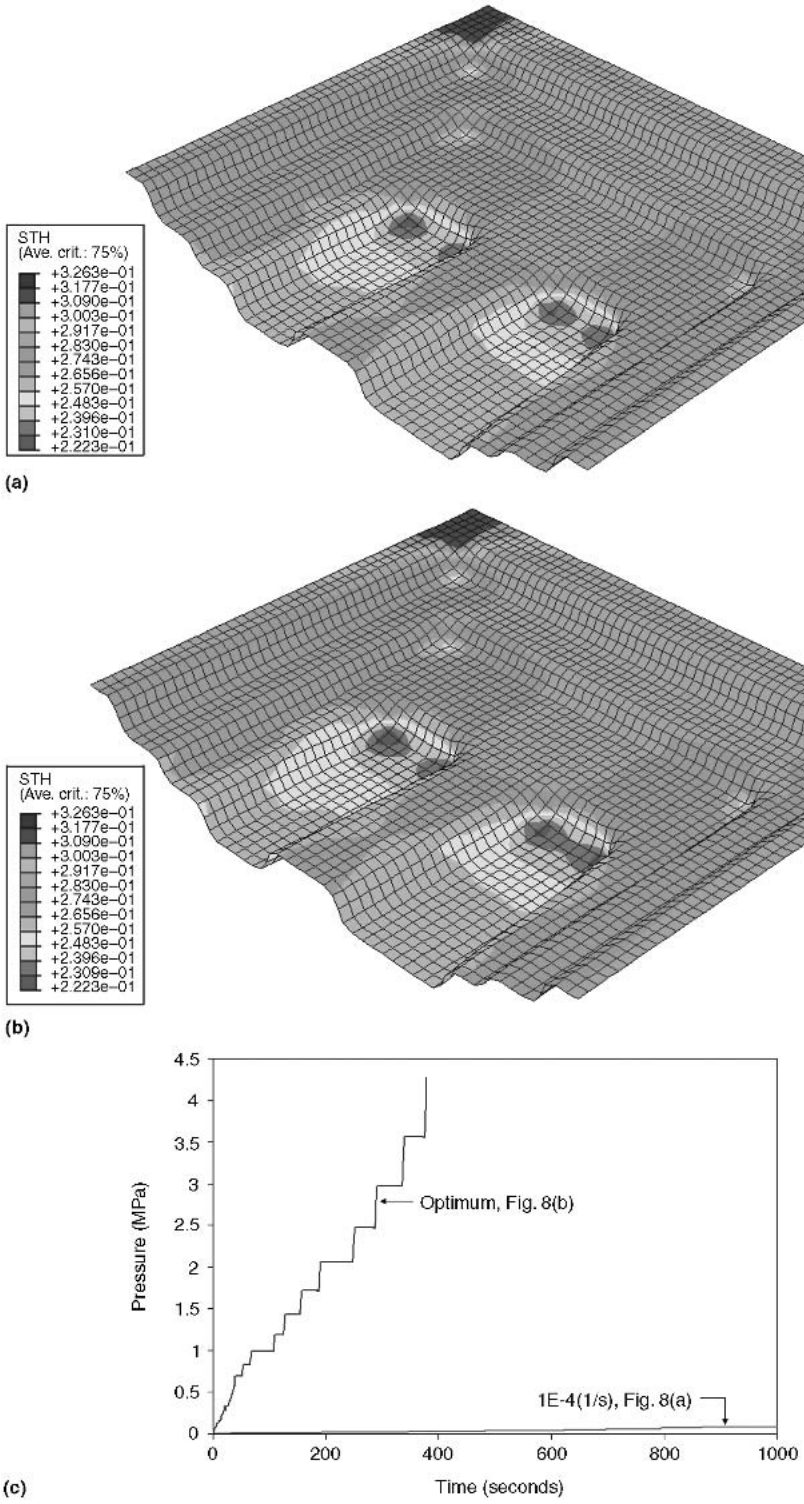

Fig. 8 Blow forming of an aircraft blowout door. (a) Thickness distribution profile for constant strain rate forming at 10^{-4} s^{-1} (forming time, 4864 s), (b) Thickness distribution profile for the optimum forming case (forming time 379 s). (c) Pressure profiles

continues and more cavitation (and necking) threatens the stability of deformation, the pressure is adjusted to a lower value. This optimization approach is based on the deformation and failure characteristics of the material and is not chosen arbitrarily.

7. Application

To demonstrate the effectiveness of the proposed optimization scheme that utilizes the microstructure-based constitutive model and the multiscale stability criterion, a numerical simu-

lation for SPF of an aircraft blowout door was performed. The main advantage of forming this part using SPF technique is to eliminate a significant number of detail parts and joining steps. Figure 7 shows the die-sheet geometry of the forming process. Due to symmetry, one-half of the assembly is used in the simulation. Due to the lack of data, the die geometry proposed here represents a simplified geometry of an actual aircraft blowout door. The die used here is 100 cm long and 64 cm wide, with a 10 cm maximum depth. The part was formed at a constant strain rate of 1×10^{-4} s^{-1} (Fig. 8a) and using the optimized strain rate scheme (Fig. 8b). The pressure profile for the two forming scenarios is shown in Fig. 8(c). The results show again the capability of the proposed optimization technique to reduce the forming time without compromising the uniform thickness distribution of the formed part. The forming time was significantly reduced from 4864 to 379 s, and the uniformity of the sheet was maintained.

8. Conclusions

A detailed FE analysis of superplastic gas-blow forming was carried out using a modified microstructure-based constitutive model that accounts for grain growth and cavitation. An optimum forming procedure was also developed using a multiscale stability criterion that accounts for both cavitation and geometrical necking. Various optimization schemes were also used and compared with the proposed optimum scheme. The results highlighted the importance of accounting for microstructure evolution during superplastic deformation, and misleading results can be generated if appropriate evolution equations for the microstructure are not used. Additionally, significant benefits and advantages can be obtained using the proposed optimization procedure. It is important to point out that the accuracy of FE simulations mainly depends on the accuracy of representation of the actual material behavior during forming. There is a need to develop more accurate evolution equations for the evolving microstructure during deformation, taking into account multiaxial stress states and anisotropy. These issues are currently under investigation.

Acknowledgment

The support of the National Science Foundation, CAREER Award No. DMI-0238712, is acknowledged.

References

1. D.G. Sanders, The History and Current State-of-The-Art in Airframe Manufacturing Using Superplastic Forming Technologies, *Advances in Superplasticity and Superplastic Forming,* E. Taleff, P. Friedman, P. Krajewski, R. Mishra, and J. Schroth, Ed., The Minerals, Metals and Materials Society, 2004, p 3-8
2. F. Jovane, An Approximate Analysis of the Superplastic Forming of a Thin Circular Diaphragm, Theory and Experiments, *Int. J. Mech. Sci.,* Vol 10, 1968, p 403-427
3. D.L. Holt, Analysis of the Bulging of Superplastic Sheet by Lateral Pressure, *Int. J. Mech. Sci.,* Vol 12, 1970, p 491-497
4. J.A. Belk, A Quantitative Model of the Blow Forming of Spherical Surfaces in Superplastic Sheet Metal, *Int. J. Mech. Sci.,* Vol 17, 1975, p 505-511
5. A. Dutta and A.K. Mukherjee, Superplastic Forming: An Analytical Approach, *Mater. Sci. Eng.,* Vol A157, 1992, p 9-13
6. X.D. Ding, H.M. Zbib, C.H. Hamilton, and A.E. Bayoumi, On the Optimization of Superplastic Blow-Forming Processes, *J. Mater. Eng. Perf.,* Vol 4 (No. 4), 1995, p 474-485
7. C.F. Yang, L.H. Chiu, and S.C. Lee, Superplastic Forming of 7475 Al Alloy by Variable-Pressure Blowing, *Scr. Mater.,* Vol 34 (No. 10), 1996, p 1555-1560
8. M.K. Khraisheh and H.M. Zbib, Optimum Forming Loading Paths for Pb-Sn Superplastic Sheet Materials, *J. Eng. Mater. Technol.,* Vol 121 (No. 3), 1999, p 341-345
9. L. Carrino, G. Giuliano, and C. Palmieri, On the Optimisation of Superplastic Forming Processes by the Finite-Element Method, *J. Mater. Proc. Technol.,* Vol 143-144, 2003, p 373-377
10. M.K. Khraisheh and F.K. Abu-Farha, Microstructure Based Modeling of Anisotropic Superplastic Deformation, *Trans. NAMRI/SME,* Vol 31, 2003, p 41-47
11. N.V. Thuarmalla and M.K. Khraisheh, Effects of Microstructural Evolution on the Stability of Superplastic Deformation, *Proceedings of the Second MIT Conference on Computational Fluid and Solid Mechanics,* K.J. Bathe, Ed., Elsevier, Vol 1, 2003, p 683-686
12. N.V. Thurmulla, P.V. Deshmukh, and M.K. Khraisheh, Multi-Scale Analysis of Failure During Superplastic Deformation, *Mater. Sci. Forum,* Vol 447-448, 2004, p 105-110
13. M. Khraisheh, H. Zbib, C. Hamilton, and A. Bayoumi, Constitutive Modeling of Superplastic Deformation. Part I, Theory and Experiments, *Int. J. Plast.,* Vol 13 (No. 1/2), 1997, p 143-164
14. C.H. Hamilton, H.M. Zbib, C.H. Johnson, and S.K. Richter, Dynamic Grain Coarsening: Its Effects on Flow Localization in Superplastic Deformation, *Second SAMPE Symposium,* Chipa, Japan, I. Kimpara, Ed., Society for the Advancement of Material and Process Engineering, Japan, 1991, p 272-279
15. J. Pilling and N. Ridely, *Superplasticity in Crystalline Solids,* The Institute of Metals, 1989, p 102-157
16. E.W. Hart, Theory of the Tensile Test, *Acta Metall.,* Vol 15, 1967, p 351-355
17. C.H. Johnson, C.H. Hamilton, H.M. Zbib, and S. Richter, Designing Optimized Deformation Paths for Superplastic Ti-6Al-4V, *Advances in Superplasticity and Superplastic Forming,* N. Chandra, H. Garmestani, and R.E. Goforth, Ed., The Minerals, Metals and Materials Society, 1993, p 3-15